

1 **Temporal modulation of the NF-κB RelA**
2 **network in response to different types of DNA**
3 **damage**

4 *Amy E. Campbell^{1†}, Catarina Ferraz Franco^{1†}, Ling-I Su², Emma K. Corbin², Simon*
5 *Perkins³, Anton Kalyuzhnyy³, Andrew R. Jones³, Philip J. Brownridge¹, Neil D.*
6 *Perkins², Claire E. Eyers^{1*}*

7 ¹ Centre for Proteome Research, Department of Biochemistry & Systems Biology, Institute of
8 Institute of Systems, Molecular & Integrative Biology, University of Liverpool, Liverpool, L69
9 7ZB, UK

10 ² Faculty of Medical Sciences, Biosciences Institute, Newcastle University, Newcastle Upon
11 Tyne, NE2 4HH, UK

12 ³ Department of Biochemistry & Systems Biology, Institute of Institute of Systems, Molecular
13 & Integrative Biology, University of Liverpool, Liverpool, L69 7ZB, UK

14

15 † These authors contributed equally to this manuscript

16 * Correspondence to ceyers@liverpool.ac.uk

1 **ABSTRACT**

2 Different types of DNA damage can initiate phosphorylation-mediated signalling cascades
3 that result in stimulus specific pro- or anti-apoptotic cellular responses. Amongst its many
4 roles, the NF- κ B transcription factor RelA is central to these DNA damage response
5 pathways. However, we still lack understanding of the co-ordinated signalling mechanisms
6 that permit different DNA damaging agents to induce distinct cellular outcomes through
7 RelA. Here, we use label-free quantitative phosphoproteomics to examine the temporal
8 effects of exposure of U2OS cells to either etoposide (ETO) or hydroxyurea (HU) by
9 monitoring the phosphorylation status of RelA and its protein binding partners. Although few
10 stimulus-specific differences were identified in the constituents of phosphorylated RelA
11 interactome after exposure to these DNA damaging agents, we observed subtle, but
12 significant, changes in their phosphorylation states, as a function of both type and duration
13 of treatment. The DNA double strand break (DSB)-inducing ETO invoked more rapid,
14 sustained responses than HU, with regulated targets primarily involved in transcription, cell
15 division and canonical DSB repair. Kinase substrate prediction of ETO-regulated
16 phosphosites suggest abrogation of CDK and ERK1 signalling, in addition to the known
17 induction of ATM/ATR. In contrast, HU-induced replicative stress mediated temporally
18 dynamic regulation, with phosphorylated RelA binding partners having roles in rRNA/mRNA
19 processing and translational initiation, many of which contained a 14-3-3 ϵ binding motif, and
20 were putative substrates of the dual specificity kinase CLK1. Our data thus point to
21 differential regulation of key cellular processes and the involvement of distinct signalling
22 pathways in modulating DNA damage-specific functions of RelA.

23

24 **Short title:** DNA damage regulation of the RelA signalling network

25

26 **Abbreviations:** ATM: ataxia telangiectasia mutated; CDK: cyclin-dependent kinase; DMSO:
27 dimethyl sulfoxide; DSB: DNA double stranded breaks; ERK: Extracellular signal-regulated
28 kinase; ETO: etoposide; HU: hydroxyurea; IR: ionising radiation; MS: mass spectrometry;
29 MS/MS: tandem mass spectrometry; PTM: post-translational modifications; UV: ultraviolet

30

31 **Keywords:** DNA damage; RelA; p65; NF- κ B; phosphorylation; Mass Spectrometry,
32 phosphoproteomics; etoposide; hydroxyurea

33

1 INTRODUCTION

2 RelA, also known as p65, is a key member of the NF- κ B family of transcription factors, which
3 serve as 'master regulators' of the cellular inflammatory and stress responses, and are key
4 components that maintain tissue homeostasis and contribute to aging. As part of a functional
5 homo- or hetero-dimer (preferentially with p50), RelA regulates a diverse set of genes
6 involved in core cellular processes such as inflammation, proliferation, apoptosis and
7 metastasis [1]. The precise functional roles (the complement of genes transcribed) of RelA
8 are governed both by its post-translational modification (PTM) status, and the transcriptional
9 complexes formed, which are themselves regulated in a co-ordinated fashion through
10 numerous cell signalling pathways [2–4]. PTMs have the potential to regulate many aspects
11 of NF- κ B signalling in response to different stimuli, including nuclear translocation, protein-
12 protein or protein-DNA interactions, and stability, often working in a combinatorial fashion to
13 regulate complex formation and transcriptional output.

14

15 While NF- κ B signalling is commonly associated with inflammation and the immune
16 response, these pathways also play key roles in the cellular response to DNA stress.
17 Consequently, aberrant NF- κ B signalling is observed in, and often a contributing factor to,
18 many human diseases, including autoimmune disorders, chronic inflammatory diseases, and
19 cancer [1,5–7]. NF- κ B signalling is also central to age-related degenerative diseases as a
20 result of accumulated age-related DNA damage [8]. The pro-survival effects mediated by
21 NF- κ B in response to specific-types of DNA damage in part explains the cellular resistance
22 to chemotherapy. Hence, a clear understanding of NF- κ B signalling in response to DNA
23 damage is important, not only in the context of ageing, but also to enhance cancer treatment
24 strategies.

25

26 In response to different types of DNA damage, cells invoke specific responses that promote
27 DNA repair, induce cell cycle arrest, regulate cell death or induce cellular senescence [9,10].
28 For example, inhibition of DNA replication using hydroxyurea (HU), which inhibits
29 ribonucleotide diphosphate reductase, arrests cells primarily in S-phase [11–15]. In contrast,
30 agents such as etoposide (ETO), which induces DNA double stranded breaks (DSBs) by
31 preventing topoisomerase II-mediated DNA re-ligation during replication and cell division,
32 cause cells to accumulate in the G2/M phase of the cell cycle [16–19]. Whilst activation of
33 NF- κ B-responsive genes following DNA stress has been investigated, the mechanisms of
34 regulating these differential outputs remain poorly characterised [1,5–7]. Both HU and ETO
35 invoke a DNA damage stress response through ataxia telangiectasia mutated (ATM)-
36 mediated activation of NF- κ B, leading to elevated levels of NF- κ B targets such as Survivin
37 and Bcl-xL. However, these two types of DNA damaging agents result in distinct cellular
38 responses in a variety of tumour-derived cell lines and in primary cells cancer cells, in part

1 due to induction of different NF- κ B gene expression patterns [19–22]; HU mediates a pro-
2 apoptotic response, while an anti-apoptotic response results following cellular exposure to
3 ETO [22]. Differential involvement of p53 in regulating NF- κ B outputs in response to these
4 different types of DNA damaging agents also plays a role: while the transcriptional response
5 to HU requires p53 for both early and late NF- κ B target gene expression, NF- κ B-mediated
6 transcription in response to ETO is independent of p53 [22].

7
8 The activity of all NF- κ B subunits, including RelA, is extensively controlled by a variety of
9 PTMs including: phosphorylation, acetylation, methylation, glycosylation, proline
10 isomerisation, cysteine oxidation and ubiquitination [23–26]. Of these, phosphorylation
11 accounts for the majority of the well-understood dynamic mechanisms of regulation, both
12 direct e.g. pSer45 modulation of DNA binding [26], and indirect e.g. pSer276, which controls
13 a number of other PTMs, including ubiquitination and thus RelA stability [2,27,28]. Of
14 relevance here, Thr505 phosphorylation has been shown to mediate pro-apoptotic effects
15 upon cisplatin-induced DNA damage [29,30]. Given the complexity of NF- κ B signalling,
16 unravelling the mechanisms by which NF- κ B subunits, particularly RelA, induce differential
17 transcriptional specificity in a context-dependent manner is challenging.

18
19 The sensitivity and versatility of mass spectrometry (MS) makes it ideal for the study
20 (identification and quantification) of dynamic PTMs and the regulated binding partners of
21 transcription factors and their transcriptional complexes. Here we utilise a label free
22 phosphoproteomics approach to map DNA damage-induced changes in RelA binding
23 partners and their phosphorylation status, in response to either HU-induced replicative
24 stress, or ETO-mediated DSB. We find that whilst RelA associated proteins remain largely
25 unchanged as a function of DNA stress, there are notable changes in the dynamics of
26 phosphorylation of the RelA-interactome as a function of treatment. These findings point
27 towards different signalling pathways directing the formation of specific RelA networks
28 dependent on the type of DNA damage that likely help direct transcriptional output and thus
29 the cellular response.

1 MATERIALS and METHODS

2 Reagents and Antibodies

3 Unless otherwise stated, general lab reagents were purchased from Sigma Aldrich and were
4 of the highest quality available. The following primary antibodies were used for
5 immunoblotting at 1/1000 dilution in 5% (w/w) BSA overnight at 4 °C: anti-RelA (sc-372,
6 Santa Cruz), anti-HA (Merck, HA-7), anti phospho-histone H2AX (#2577, Cell Signalling),
7 anti-PAK4 (#3242, Cell Signaling Technologies), anti-Karyopherin- β 1 H-7 (sc-137016, Santa
8 Cruz). Secondary anti-rabbit IgG (7074S, Cell Signalling Technology) was used at 1/5000
9 dilution following membrane incubation with VeriBlot (1/400 dilution, ab131366 Abcam).

11 Generation and culture of HA-RelA U2OS cells

12 The HA-RelA U2OS cell line was generated by transfecting wild-type U2OS cells with the
13 plasmid pRcRSV HA RelA plasmid, which also expresses the neomycin gene. Cells stably
14 expressing HA tagged RelA were then selected by treatment with G418 (600 μ g/mL, Melford
15 Chemicals, cat. no. G0175), with pooled populations of cells used in experiments.

17 Cell treatment and lysis

18 U2OS cells expressing HA-RelA (or HA control cells) were cultured in DMEM supplemented
19 with 10% (v/v) fetal bovine serum, penicillin (100 U/mL), streptomycin (100 U/mL), and L-
20 glutamine (2 mM) at 37 °C, 5% CO₂. Once 80% confluence was reached, cells were treated
21 with either 50 μ M etoposide (50 mM stock solution in DMSO) or 2 mM hydroxyurea (100 mM
22 stock solution in DMEM, 5% DMSO), by addition to the culture media, for the indicated
23 times. Control cells were grown for the maximum time (2 h) in 0.1% (v/v) DMSO. After
24 removal of the media, cells were washed three times with ice cold PBS. For proteomics
25 analysis, cells were harvested in 400 μ L of lysis buffer (100 mM Tris-HCl pH 8.0, 150 mM
26 NaCl, 0.5 mM EDTA, 0.5% (v/v) Triton X-100, 0.5% (v/v) NP-40, 1 x PhosSTOP™
27 phosphatase inhibitor cocktail tablet (Roche), 1 x cComplete™ Protease Inhibitor Cocktail
28 (Roche), 50 U/mL of benzonase) into 1.5 mL microtubes using a cell scraper. Cells were
29 then incubated on ice for 120 min to permit cell lysis to occur. Cell lysates were then cleared
30 by centrifugation (16,000 x g, 10 min, 4°C) and protein concentration was determined using
31 the Bradford assay. A total protein amount of 4 mg was set aside for HA-RelA
32 immunoprecipitation. Cell treatment and lysis was performed in triplicate to obtain three
33 independent biological replicates for each treatment condition and control (untreated) cells
34 for proteomics analysis.

35 For the RelA co-immunoprecipitation studies, HA-RelA or HA control U2OS cells were lysed
36 in IP lysis buffer (25 mM Tris pH 8, 0.15 M NaCl, 0.1% (w/v) NP-40, 1 mM EDTA, 1 mM
37 DTT, containing 1 x PhosSTOP™ phosphatase inhibitor cocktail tablet (Roche), and
38 cComplete™ Protease Inhibitor Cocktail (Roche)) after treatment with either ETO or HU as

1 above. Protein concentration was determined using a BCA protein assay kit according to the
2 manufacturer's instructions (Thermo Scientific).

3

4 **Immunoprecipitation of HA-RelA for proteomics**

5 Pierce™ Anti-HA Magnetic Beads were washed with 0.05% (v/v) TBST and then with lysis
6 buffer prior to addition of 4 mg cleared cell lysate (at a ratio of beads to protein of 1:2000).
7 Beads and lysate were incubated overnight using an end-over-end rotor at 4°C. Beads were
8 then collected using a magnetic stand and washed three times with wash buffer (40 mM
9 Tris-HCl pH 8.0, 0.1% (v/v) NP-40, 1 mM EGTA, 6 mM EDTA, 6 mM DTT, 0.5 M NaCl, 1 x
10 PhosSTOP™ phosphatase inhibitor cocktail tablet (Roche), 1 x cOmplete™ Protease
11 Inhibitor Cocktail (Roche)); one time with HPLC grade water and finally, three times with 25
12 mM ammonium bicarbonate (AMBIC). To recover the immunoprecipitated material, the
13 beads were resuspended in 100 µL of 25 mM AMBIC to which 6 µL of a 1% (w/v) solution of
14 RapiGest (Waters, UK) in 25 mM AMBIC was added. Samples were then heated to 80 °C for
15 10 min. Supernatants containing the eluted proteins were recovered using a magnetic stand
16 and used for in-solution digestion.

17

18 **Co-immunoprecipitation of HA-RelA and immunoblotting**

19 Pierce™ protein A/G Magnetic Beads were incubated with anti-HA antibody (sc-7392, Santa
20 Cruz Biotechnology) in 5% (w/w) BSA for 3 hr at 4°C, using 10 µL beads and 1 µg antibody
21 per IP. Beads were washed three times with IP lysis buffer (500 µL) and incubated overnight
22 using an end-over-end rotor at 4°C. Beads were then collected using a magnetic stand and
23 washed three times with wash buffer prior to elution of bound protein in 30 µL of 2x SDS
24 loading buffer for SDS-PAGE and immunoblotting.

25

26 **In-solution digestion and TiO₂-based enrichment of phosphorylated peptides**

27 Samples were digested with trypsin and subjected to TiO₂-based phosphopeptide
28 enrichment as previously described [31]. In brief, disulfide bonds were reduced by addition
29 of DTT to a final concentration of 4 mM (10 min, 60 °C with gentle agitation). Samples were
30 cooled to room temperature and free cysteines alkylated with 14 mM iodoacetamide (30 min,
31 RT), prior to addition of DTT (to 7 mM final) to quench excess iodoacetamide. Samples were
32 digested with trypsin (1:50 trypsin:protein ratio) overnight at 37°C with light agitation (450
33 rpm on a Eppendorf thermomixer). Digestion was stopped by the addition of trifluoroacetic
34 acid (TFA) to a final concentration of 0.5% (v/v) and incubated for 45 min at 37°C. RapiGest
35 insoluble hydrolysis products were removed by centrifugation (13 000 x g, 15 min, 4°C).
36 Digested samples were dried by vacuum centrifugation and resolubilized in TiO₂ loading
37 buffer (80% acetonitrile, 5% TFA, 1 M glycolic acid) to achieve a peptide concentration of 1
38 µg/µL and sonicated for 10 min. TiO₂ beads (50 µg/µL in loading buffer) were mixed at 1400

1 rpm (with intermittent vortexing to prevent the beads from pelleting) with the resuspended
2 peptides (bead:protein ratio of 5:1) for 20 min at RT. TiO₂ beads were recovered by
3 centrifugation (2000 x g, 1 min) and washed successively for 10 min (1400 rpm) with 150 µL
4 of loading buffer, 80% acetonitrile 1% TFA, then 10% acetonitrile, 0.2% TFA. Prior to elution,
5 beads with bound phosphopeptides were dried to completion by vacuum centrifugation.
6 Bound phosphopeptides were then eluted by addition of 100 µL of 1% (v/v) ammonium
7 hydroxide and then with 100 µL of 5% (v/v) ammonium hydroxide. Both elutions were
8 combined and dried by vacuum centrifugation.

10 **Liquid chromatography-tandem mass spectrometry (LC-MS/MS) analysis**

11 Phosphopeptide enriched samples were analysed by LC-MS/MS using an Ultimate 3000
12 RSLC™ nano system (Thermo Scientific, Hemel Hempstead) coupled to a QExactive HF
13 mass spectrometer (Thermo Scientific). The samples were loaded onto a trapping column
14 (Thermo Scientific, PepMap100, C18, 300 µm X 5 mm), using partial loop injection, for
15 seven minutes at a flow rate of 4 µL/min with 0.1% (v/v) FA, and resolved on an analytical
16 column (Easy-Spray C18 75 µm x 500 mm 2 µm column) using a gradient of 97% A (0.1%
17 formic acid), 3% B (99.9% ACN 0.1% formic acid) to 60% A, 40% B over 80 minutes at a
18 flow rate of 300 nL/min. Data-dependent acquisition employed a 60,000 resolution full-scan
19 MS scan (MS1) with AGC set to 3e6 ions with a maximum fill time of 100 ms. The 10 most
20 abundant peaks were selected for MS/MS using a 60,000 resolution scan (AGC set to 1e5
21 ions with a maximum fill time of 100 ms) with an ion selection window of 1.2 m/z and a
22 normalised collision energy of 29. A 20 sec dynamic exclusion window was used to minimise
23 repeated selection of peptides for MS/MS.

25 **LC-MS/MS data analysis**

26 LC-MS/MS files were aligned in Progenesis Q1 for Proteomics label-free analysis software.
27 At this stage, no normalisation was performed and an aggregate file containing raw
28 abundances from all the peaks across all runs was exported from Progenesis. These files
29 were searched against UniProt Human reviewed protein database (downloaded December
30 2015; 20,187 sequences) using MASCOT (v 2.6) within Proteome Discoverer (v. 1.4;
31 Thermo Scientific). Parameters were set as follows: MS1 tolerance of 10 ppm, MS2 mass
32 tolerance of 0.01 Da; enzyme specificity was defined as trypsin with two missed cleavages
33 allowed; Carbamidomethyl Cys was set as a fixed modification; Met oxidation, and
34 Ser/Thr/Tyr/His phosphorylation were defined as variable modifications. Data were filtered to
35 a 1% false discovery rate (FDR) on peptide spectrum matches (PSMs) using automatic
36 decoy searching with MASCOT. *ptmRS* node with Proteome Discoverer was used to
37 determine phosphosite localization confidence. To match *ptmRS* scores to Progenesis
38 MASCOT output files, two rounds of Excel vlookup functions were used: 1) to retrieve scan

1 numbers from the TOP hit per feature number, and 2) to retrieve *ptmRS* score using the
2 corresponding scan number.
3 'Normalizer' software [32] was used to assess the suitability of various types of
4 normalization strategies on the data. Amongst normalization strategies, VSN-G (group-
5 based variance stabilizing normalisation) performed well under various quality control
6 metrics indicating a reduction in technical variance. The 'vsn' R/Bioconductor package [33]
7 was then used to normalize log transformed peptide abundance data for the subsequent
8 stages of analysis. Pairwise t-test and cross condition ANOVA statistical testing, followed by
9 Benjamini-Hochberg global correction was subsequently also performed in R for any
10 replicate groups without missing values. Unless otherwise described, all plots were
11 generated in R.

12

13 **Network analysis**

14 All proteins with quantified phosphopeptides in two or more (of the three) repeats of any
15 condition were combined for network analysis of RelA-associated proteins. Common
16 contaminants that bind non-specifically in IP experiments were removed by filtering protein
17 accessions against a CRAPome database (<https://www.crapome.org>) [34] of contaminants
18 observed with Streptactin-HA IPs from U2OS cells (CC405, CC406 and CC410). All proteins
19 not present in the contaminant database were entered into STRING (<https://string-db.org>,
20 v11.0) to generate a network of protein associations [35]. The generated network was
21 filtered to contain only high confidence associations (interaction score ≥ 0.7) with
22 experimental or database evidence only. Proteins with no high confidence interactions were
23 removed from the network and the remaining nodes were clustered using the Kmeans
24 algorithm (K=9). The resulting network was imported into Cytoscape [36] with nodes
25 recoloured, grouped into the top 9 Kmeans clusters and node shapes for proteins unique to
26 HU or ETO changed to squares or diamonds respectively. For the top 9 Kmeans clusters,
27 nodes corresponding to proteins with differentially regulated phosphopeptides in response to
28 either HU, ETO or both treatments, with respect to the untreated control, were outlined in
29 red, blue or black respectively.

30

31 **Functional enrichment analysis**

32 All functional enrichment analysis was performed using the functional annotation tool in
33 DAVID (<https://david.ncicrf.gov>, v6.8) against a background of the human proteome [37,38].
34 For biological process GO term pie charts, all significantly enriched (Benjamini adj.*p*-value \leq
35 0.05) GO biological process terms, with associated Benjamini adj.*p*-values, were
36 summarised using REVIGO [39] then visualised with the CirGO Python package [40].
37 Bubble plots including significantly enriched (Benjamini adj.*p*-value \leq 0.05) GO biological

1 process (BP), molecular function (MF), cellular component (CC) and overrepresented
2 keywords, filtered to remove duplicate terms, were plotted in R.

3

4 **Kinase Prediction/Sequence motif analysis**

5 Kinase-substrate prediction for all differentially regulated (t -test, $p \leq 0.05$) phosphosites was
6 performed using NetPhorest [41,42]. Briefly, for all 'class I' phosphorylation sites ($ptmRS$
7 ≥ 0.75) protein identifiers together with the position of the phosphorylated residue were
8 submitted to NetPhorest using the high-throughput web interface, with the top scoring
9 prediction for each site reported. Kinase predictions were summarised for all up- or down-
10 regulated phosphosites with the resulting data plotted in R. For sequence motif analysis,
11 sequence windows encompassing 7 amino acids either side of the phosphorylated residue
12 were extracted for all phosphosites significantly up- or down- regulated (t -test, $p \leq 0.05$) with
13 respect to the untreated control. Consensus sequence motifs were generated with iceLogo
14 v1.2 [43] against a background of the precompiled human Swiss-Prot composition using
15 percent difference as the scoring system and a p -value cut-off of 0.05. The most confident
16 phosphosite per phosphopeptide was also cross-referenced against data from PeptideAtlas
17 (PA) [64] (2020 build), and from PhosphoSitePlus (PSP) [65] (11/03/20 build), categorising
18 phosphorylation site confidence based on the number of observations - "High": ≥ 5 previous
19 observations, very likely true site; "Medium": 2-4 previous observations, likely true site;
20 "Low": 1 previous observation, little support that it is a true site; PA only - "Not
21 phosphorylated": frequently (>5) observed to be not phosphorylated, never observed as
22 phosphorylated; "Other" - no confident evidence in any category. Observations in PA were
23 counted with a threshold of >0.95 PTM Prophet probability for positive evidence, and ≤ 0.19
24 for evidence of not being phosphorylated.

25

1 RESULTS

2 Selection of DNA damage timepoints

3 To identify changes in the phosphorylation status of RelA and its protein binding partners in
4 response to different types of DNA damage, we first examined the kinetics of DNA damage
5 after treatment with either the DSB inducer ETO, or the replicative stress inducer HU in the
6 HA-RelA U2OS cell line. Using gamma-H2AX as a marker [44,45], we observed rapid DNA
7 damage (within 30 min) following treatment with either ETO or HU (Fig. 1; Supplementary
8 Fig. 1). Gamma-H2AX levels peaked faster with ETO than HU, but sustained (and maximal)
9 levels were observed with both agents following ~ 2 hours of continuous treatment. A time-
10 course of the effect of these different DNA damaging agents on the RelA phosphorylation
11 interactome was therefore evaluated by treatment of the HA-RelA U2OS cells with either
12 ETO or HU for 0, 30, 60 or 120 minutes prior to immunoprecipitation (IP) of the HA-tagged
13 RelA. Immunoprecipitated proteins were subject to titanium dioxide (TiO₂)-based
14 phosphopeptide enrichment prior to LC-MS/MS with label-free peptide quantification (Fig. 1).

15

16 Network of RelA-associated proteins

17 Using the identified (phospho)peptides as proxy for protein identifications, the list of RelA
18 bound proteins under all conditions was filtered against a 'CRAPome' database of
19 contaminants commonly observed in Streptactin-HA IPs from U2OS cells (CC405, CC406
20 and CC410), which provided the closest match to the experimental workflow described here.
21 Phosphopeptide quantification data was normalised and subjected to ANOVA testing across
22 all conditions, and individual t-tests across all pairs of conditions. Using this list, the temporal
23 effect of treatment with either ETO or HU on RelA bound phosphoproteins was evaluated for
24 all those proteins quantified in at least 2 biological replicates, under a given condition.

25 To generate a network of high confidence interactors, the remaining 815 RelA-associated
26 proteins combined across all conditions (Supp. Table 1) were inputted into STRING (v11.0)
27 [35] using experimental and database sources only, and clustered using the Kmeans
28 algorithm (k=9). Twelve of these proteins failed to yield high confidence interactions and
29 therefore were filtered out of subsequent datasets (Fig. 2). Gene Ontology (GO) enrichment
30 analysis of biological function for these 803 proteins within the top 9 network clusters
31 confirmed association of RelA with a number of IκB kinase/NF-κB signalling proteins (Fig.
32 2A), including RelB, c-Rel, p105/p50, p100/p52, IκBα, IκBβ, and the DNA damage response
33 (Fig. 2B). Clusters of proteins across a number of core cellular processes were also
34 identified in the RelA interactome, including key proteins involved in cell division,
35 transcriptional regulation, mRNA/rRNA processing and MAPK/ERK/VEGF signalling (Fig. 2
36 [A-H]). Amongst these interactions partners, we also confirmed observation of a number of
37 known RelA binding proteins, including *e.g.* replication factor C (RFC1), p300, SP1 and
38 HDAC6 [46–49].

1 To determine the temporal response in the RelA interactome of phosphorylated proteins to
2 the different DNA damaging agents, we evaluated those quantified proteins exhibiting a
3 statistically significant (t-test, $p \leq 0.05$) change in response to time-dependent treatment with
4 ETO or HU, in comparison to control (DMSO treated) cells. Interestingly, the constituents of
5 the RelA interactome changed very little in response to DNA damage, with the vast majority
6 of the phosphoproteins identified being observed before and after exposure to either ETO or
7 HU (round nodes, Fig. 2). Of the 803 protein binding partners with high confidence
8 interactors, only 7 were unique to ETO (diamond nodes, Fig. 2; Table 1), while 8 were
9 specific to HU (square nodes, Fig. 2; Table 1).

10 Of the 7 ETO-specific proteins identified in this network, three are essential components of
11 the ERK/MAPK signalling pathway: the protein kinases ERK1 and PAK, and DUSP9, a dual
12 specificity phosphatase that preferentially targets the MAPK/ERK family. A fourth member of
13 this ETO-specific cohort, AAED1 (which has no known common confident interactors and is
14 therefore not represented in Fig. 2), is also reported to positively regulate the ERK/MAPK
15 (and AKT1) pathway, ultimately leading to upregulation of hypoxia-inducible factor (HIF)-1 α
16 and enhanced glycolysis [50]. In contrast, the 8 HU-specific proteins exhibited diverse
17 biological functions, with only one of these proteins, nucleoprotein TPR, falling into one of
18 the top 8 network clusters (Fig. 2A).

19 In support of the RelA protein networks defined in these proteomics experiments, we
20 confirmed PAK4 as a novel ETO-regulated RelA binding partner by co-immunoprecipitation,
21 with PAK4 binding occurring maximally in these experiments after 60 min treatment with
22 ETO (Fig. 3). No discernible increase in PAK4 binding was observed in response to cellular
23 treatment with HU.

24 Also highlighted in the nodes of the top 8 network clusters are the proteins for which we
25 identified statistically significantly differentially regulated phosphopeptides (t-test, $p \leq 0.05$) in
26 response to treatment with either ETO or HU (or both) with respect to the (DMSO treated)
27 control cells (Fig. 2 [A-H]; Supp. Table 3). Interestingly, the proteins with differentially
28 regulated phosphopeptides following either ETO or HU treatment are largely distinct
29 between the two types of DNA damaging agents, and are interspersed across the network
30 clusters rather than being specific to certain functional biological groups (Supplemental
31 Figure 2-gifs). These data thus suggest that whilst there was relatively little change in the
32 RelA-associated phosphoproteins as a function of DNA damage, the phosphorylation states
33 of those associated proteins were dependent on both the type and duration of the induced
34 DNA damage response.

35

36 **RelA is minimally differentially phosphorylated in U2OS cells in response to ETO or** 37 **HU treatment**

38 Looking specifically at RelA, we observed good sequence coverage of the N-terminal region
39 (>70%; 46% overall; Supp. Fig. 3), allowing us to quantify most of the known

1 phosphorylation sites in the *N*-terminal half of the protein including; Ser42, Ser45, Ser131,
2 Ser203/Ser205, Ser238, Ser240 and S316. Two novel phosphorylation sites at Thr54 and
3 Ser169 were also observed (Supp. Fig. 3). No phosphorylation sites were confidently
4 identified in the *C*-terminus of RelA containing the transactivation domains (TAs), in part due
5 to the limited ability to generate suitable tryptic peptides for analysis (as documented
6 previously [26]). Although phosphopeptides covering the extreme *C*-terminus (from residue
7 503 and including the known sites of phosphorylation at T505, S529 and S536) were
8 observed, the site of phosphorylation could not be unambiguously defined.
9 Overall, the changes observed in RelA phosphorylation in response to DNA damage under
10 these conditions were very limited. Only Ser131 was statistically significantly regulated by
11 both the DSB-inducing ETO and HU: pSer131 increased marginally by 1.03-fold (with
12 respect to the DMSO-treated control) at 120 min (p -value = 0.047) in response to ETO,
13 responding much more rapidly to HU, increasing 1.05 fold by 30 min (p -value = 0.046),
14 decreasing slightly (although not statistically) by 60 min, and returning to baseline levels by
15 120 min. We have previously shown that this site is also responsive to TNF α treatment of
16 U2OS cells, and phosphorylated *in vitro* by IKK β , in a manner that is significantly enhanced
17 in the presence of the RelA dimerization partner, p50, and reduced in the presence of I κ B α
18 [26]. In contrast, Ser45, a phosphorylation site that we previously demonstrated plays a
19 critical role in reducing the ability of RelA to bind to DNA (alongside Ser42, which was not
20 observed in the HU-treated cells) [26], was reduced by 1.1 fold (p -value < 0.01) 60 min after
21 cellular treatment with HU, suggesting an HU-mediated regulation of RelA transcription, in
22 part through Ser45 phosphorylation (Supp. Fig. 3).

23

24 **ETO and HU induced different phosphorylation dynamics in the RelA network**

25 Of the 696 proteins identified in the RelA network in the presence of ETO, 184 exhibited
26 ETO-dependent changes in phosphorylation status, with a total of 312 phosphopeptides
27 exhibiting a statistically significant change. GO term analysis of biological processes of these
28 184 proteins revealed enrichment primarily of proteins involved in transcription (p < 0.001),
29 RNA processing (p < 0.001), cell division (p < 0.001) and, unsurprisingly, the DNA damage
30 response (p < 0.001) (Fig. 4A). Slightly fewer changes arose in response to HU, with 235
31 phosphopeptides from 157 proteins exhibiting a statistically significant change compared to
32 control (Fig. 4B), those primarily being involved in translation (p < 0.001) and rRNA
33 processing (p < 0.001). Interestingly, only 37 of the proteins exhibiting dynamic changes in
34 response to treatment were common between the two types of DNA damaging agent,
35 indicating significant differences in the mechanisms whereby RelA mediates the outputs
36 from these two DNA damaging agents (Fig. 4C). For each of the phosphorylation sites
37 identified in these experiments, we also determined if they had been observed previously in
38 either PhosphositePlus (PSP), or Peptide Atlas (PA), categorising our quantified

1 phosphosites based on the number of prior observations (Tables S2, S3). Of the ~3,100
2 unique phosphorylation sites identified in these studies, ~70% have been previously
3 observed at medium or high confidence in PSP, having been observed at least twice
4 previously. Of those phosphorylation sites that were dynamically regulated (with statistical
5 significance) in response to cellular treatment with either of these DNA damage agents, 86%
6 and 93% (for ETO and HU respectively) have been reported previously.

7 We next evaluated the temporal dynamics of these phosphorylation changes as a function of
8 treatment type (Fig. 4D). Intriguingly, ETO and HU induced very different dynamics in
9 phosphosite regulation. Indeed, approximately one-quarter (~70 phosphopeptides) of the
10 ETO-regulated phosphopeptides, were responsive within 60 min of treatment, with the
11 change in phosphorylation status being maintained over the duration of the 120 min
12 experiment (Fig. 4D, E). In contrast, only 8% (~20 phosphopeptides) of HU-dependent
13 phosphorylation changes occurred within the first 60 min and were then sustained for the
14 duration (Fig 4D, F). Overall, HU-mediated phosphorylation changes were much more
15 dynamic, with 39% of the phosphopeptides quantified in these experiments significantly
16 regulated (being observed at either increased, or reduced levels), before reverting back,
17 either to control levels, or in some instances, in the opposite direction. Just over half of those
18 phosphopeptides that were differentially regulated by either ETO or HU did not exhibit a
19 statistically significant change until after more than 60 min of continuous treatment, *i.e.* they
20 were late responders that were only observed in these experiments 120 min after exposure
21 (Fig. 4D).

22

23 **Phosphorylation of RelA-associated proteins in response to etoposide**

24 Of the 312 phosphopeptides that were differentially regulated by ETO (with respect to the
25 untreated control ($p \leq 0.05$)) across all time-points, 151 increased in abundance, while 159
26 were down-regulated (Supp. Table 2). Only two phosphorylation sites exhibited significant
27 temporal dynamics (with levels being significantly elevated or decreased at sequential time-
28 points), although the selective nature of the timing at which these measurements were made
29 could be masking additional dynamics. Overall, the relative fold change in phosphopeptide
30 abundance (up- or down-) was relatively small, with the greatest statistically significant fold
31 change being ~1.4 (Fig. 5A-C; Supp. Table 2). 14 phosphopeptides were quantified in all
32 three biological replicates for a given ETO condition but absent in control cell lysates. As the
33 fold-change in relative abundance could thus not be defined for these phosphopeptides, they
34 are not represented on the volcano plots in Fig. 5A.

35 In-depth functional enrichment analysis of proteins that were either up- or down-regulated
36 following ETO exposure revealed some key differences in terms of the biological functions
37 that were regulated (Fig. 5D). RelA-associated proteins with an ETO-mediated reduction in
38 phosphopeptide levels showed significant enrichment for GO terms including mitosis,

1 chromatin regulation (including H4-K16 acetylation), transcriptional regulation and DNA
2 damage repair (Fig. 5D). pSer780 on MDC1, the Mediator of DNA damage checkpoint
3 protein 1, exhibited the greatest down-regulation of all phosphosites in response to ETO
4 across the time-points investigated (1.3-fold down; $p = 1.95E-04$) (Supp. Table 2, Fig. 5A-C).
5 This phosphorylation site has previously been identified as being induced in response to
6 ionising radiation (IR) [51] and ultraviolet (UV) radiation [52], both of which induce DSB,
7 although the physiological function of this phosphorylation site has not yet been defined. We
8 show here that the proportion of Ser780 phosphorylated MDC1 that contributes to the RelA
9 interactome decreases in response to ETO, suggesting that DNA-damage induced pSer780
10 may serve to disrupt the interaction of MDC1 with RelA transcriptional complexes.

11

12 It is interesting to note that many more phosphopeptides were significantly upregulated than
13 were decreased in the RelA interactome in response to ETO, particularly in the later time
14 points. Transcriptional regulation and DNA damage repair were also among the GO terms
15 enriched for those proteins with up-regulated phosphorylation sites. However, there was only
16 an ~8% overlap in common proteins with differentially regulated (up or down in response to
17 ETO) phosphopeptides (Supp. Table 2), suggesting co-ordinated regulation of these key
18 processes largely through different protein effectors rather than differential phosphorylation-
19 mediated regulation of the same proteins. Also among the GO terms enriched in the list of
20 proteins with up-regulated phosphopeptides in response to ETO were mRNA processing,
21 ATP binding, transcription corepressor functionality and type I interferon production,
22 including the NF- κ B signalling proteins (RelA (pSer131), NFKB1 (p105/p50)
23 (pSer923;Ser927) and NFKB2 (p100/p52) (pSer858, pTyr868 and pSer870), with pSer619
24 on the RNA helicase DDX41 and pSer3205 on the DNA-dependent protein kinase PRKDC
25 (Fig. 5D). Multiple phosphopeptides from the transcription factor zinc finger protein 281
26 (ZNF281/GZP1/ZBP99), containing pSer395 ($p = 2.1E-02$), pSer620 ($p = 1.1E-04$), pSer785
27 ($p = 1.9E-06$) and pSer807 ($p = 1.7E-03$), were significantly upregulated across all time
28 points (between 1.2-1.4-fold) in the RelA interactome in response to ETO, but not in
29 response to HU. ZNF281 has recently been reported to be recruited to DSBs, following
30 interaction of its zinc finger domain with XXCR4 [53], where it plays an important role in
31 non-homologous end-joining upon DNA damage, and consequently the maintenance of cell
32 viability. Supporting our findings of increased phosphorylation in response to DSB, these
33 authors also reported a slight reduction in the recruitment of a non-phosphorylatable
34 S785A/S807A ZNF281mutant to sites of DNA damage. Based on our data, we would
35 suggest that phosphorylation of ZNF281 on Ser395 and Ser620 may also be required for its
36 optimal recruitment to DNA lesions and subsequent DNA repair.

37 In an attempt to understand the signalling pathways and possible kinase-substrate
38 relationships feeding into the ETO-dependent changes in phosphorylation of the RelA-

1 binding partners, the 'class I' localized phosphosites ($ptmRS \geq 0.75$) with p -value ≤ 0.05 were
2 used as input sequences for the NetPhorest kinase-substrate prediction algorithm [34,35]
3 (Fig. 5E). Of the 117 down-regulated and 107 up-regulated phosphorylation sites that
4 passed the above thresholds, NetPhorest gave kinase-substrate predictions for 37 and 32
5 sites respectively. Among the down-regulated sites, the CDKs had the highest number of
6 predicted substrates (14, 38%), accounting at least partially, for the notable enrichment
7 across all the ETO down-regulated phosphorylation sites for Pro in the +1 position with
8 respect to the site of phosphorylation [54] (Fig. 5F). Although CDK1 was defined by
9 NetPhorest as the most likely regulator of these substrates (Table S2, Fig. 5), it should be
10 noted that the overlapping substrate specificity of CDK1/2/3/5 means that it is not possible to
11 differentiate substrates of the different CDK family members. The identification of four
12 predicted substrates for ERK1 (MAPK3), which is also a Pro-directed protein kinase [55],
13 likely also contributes to the identified sequence motif, and correlates with our observations
14 of this enzyme, and importantly, a cognate phosphatase, DUSP9, in the RelA network under
15 these conditions.

16 IceLogo sequence analysis of the ETO up-regulated phosphosites showed significant
17 enrichment for Gln (and to a lesser extent Pro) at the +1 position with respect to the site of
18 phosphorylation (Fig. 5G). Positions +2 to +5 also exhibited a strong preference for acidic
19 residues (Asp/Glu), consistent with observation of 14 predicted substrates for casein kinase
20 II alpha (CK2 α 2) in the NetPhorest output (Fig. 5E). Perhaps not surprisingly given its
21 somewhat promiscuous substrate repertoire, and an involvement in diverse cellular
22 processes (including regulation of numerous transcription factors such as NF- κ B), CK2 α 2
23 was also predicted as the regulatory enzyme for a number of the significantly down-
24 regulated phosphorylation sites. The striking observation of Gln at +1 in 36 of the up-
25 regulated phosphorylation sites (Fig. 5G) is in agreement with previous reports of ATM/ATR-
26 dependent regulation of the RelA NF- κ B pathway in response to DSB (albeit following
27 cellular exposure to TNF α rather than etoposide) [56]. ATM/ATR kinases are well known to
28 preferentially phosphorylate Ser/Thr residues following by a Gln, with substrates often
29 containing several closely spaced SQ/TQ motifs in regions termed SQ/TQ cluster domains
30 (SCDs) [57]. Whilst just 7 of the 36 SQ motif-containing sequences were predicted by
31 NetPhorest to be ATM sites, it is possible that many more of the differentially regulated
32 phosphosites that match to this consensus are potential ATM/ATR substrates, given the
33 limitations of prediction software. While phosphorylation at any given site can be induced by
34 more than one protein kinase in cells, the NetPhorest algorithm is best used as a guide and
35 will only assign a single potential enzyme, based on the best fit, and is therefore not fully
36 representative of cellular possibilities.

37 **Phosphorylation of RelA-associated proteins in response to hydroxyurea**

1 Upon HU treatment, 235 phosphopeptides from 157 proteins in the RelA interactome
2 network were significantly differentially regulated with respect to the DMSO treated control (p
3 ≤ 0.05 ; Fig. 6A-C). Of those, 121 phosphopeptides increased in abundance, while levels
4 reduced for 109 phosphopeptides. Among the phosphorylation sites exhibiting a dynamic
5 response over the time-course of HU treatment, five showed a bi-directional response,
6 increasing in some time points, but reducing in others, with respect to control levels (Supp.
7 Table 3). Only seven phosphopeptides were quantified in all three biological replicates at a
8 single HU time point that were not observed in the control cell extracts.

9

10 RelA-associated proteins with statistically significantly reduced phosphopeptide levels in
11 response to HU-mediated DNA damage were notably enriched for GO terms encompassing
12 ribosome biogenesis, mRNA processing and translation (Fig. 6D). Notably, whilst translation
13 was enriched among the proteins effected by HU treatment there was no significant
14 enrichment for proteins involved in translation with ETO. In contrast, elevated
15 phosphopeptide levels were observed for processes such as chromatin regulation and
16 chromosomal rearrangement, and to a lesser extent, transcriptional regulation and mitosis
17 (Fig. 6D). Whilst transcriptional regulation was among the GO terms enriched in response to
18 HU, it was only marginally enriched, and with a much lower significance than our
19 observations with ETO, suggesting a more much limited effect on transcriptional regulation
20 with HU than with ETO (Fig. 5D, Fig. 6D).

21

22 In agreement with the γ H2Ax immunoblotting data (Fig. 1B) which indicated a slower cellular
23 response to HU than ETO (see the heatmaps in Fig. 4F), very few significant changes in
24 phosphopeptide abundance were observed 30 min after treatment with HU (Fig. 6A).
25 Interestingly, the NFKB2 (p100) peptide phosphorylated on either Ser858/Thr859 (site
26 ambiguous) exhibited the greatest increase of any phosphopeptides at this time point, with a
27 1.4-fold change (Supp. Table 3; being observed in two charge states) (Fig. 6B). This
28 increase in HU-mediated phosphorylation is supported by additional quantification of a
29 smaller peptide in which the site of phosphorylation was defined as Ser858 (Supp. Table 3),
30 a site which was also significantly upregulated following exposure to ETO (Supp. Table 2).
31 Of note, these peptides (and others in the C-terminus of p100 that are differentially regulated
32 in response to treatment) are specific to p100, rather than the transcriptionally active p52
33 cleavage product, suggesting DNA damage-mediated regulation of either p100 processing,
34 or its ability to bind (directly or indirectly) to RelA.

35

36 The second most differentially elevated phosphopeptide after 30 (and 60) min treatment with
37 HU was the doubly phosphorylated pThr185/pTyr187-containing peptide from ERK2. This
38 phosphopeptide lies in the kinase activation loop and phosphorylation of both of these sites

1 is required for catalytic activation of ERK2 [58,59]. An early consequence of HU treatment
2 on the RelA interactome network thus appears to be activation of bound ERK2, which
3 contrasts with our observations with ETO, where there were no significant changes induced
4 in MAPK1/ERK2 phosphopeptides. Together, these findings are curious in light of the fact
5 that the C-terminal region of p100 is reported to bind to inactive ERK2, thereby preventing its
6 phosphorylation and nuclear translocation. The fact that we observe increased
7 phosphorylation of ERK2 alongside phosphorylation in the C-terminal 'death domain' of p100
8 may suggest a role for these p100 phosphorylation sites in regulation its ability to interact
9 with ERK2 [60].

10

11 Nibrin, a member of the MRN complex which plays a critical role in DSB repair and cell cycle
12 checkpoint control, also exhibited elevated Ser343 phosphorylation by 30 min HU treatment.
13 Interestingly, the pSer343 site observed falls within an SQ motif which has previously been
14 shown to be phosphorylated by ATM in response to IR, and is believed to play a role in intra-
15 S phase checkpoint activation [61,62] (Fig. 6A and 6E). This same phosphorylation site was
16 also rapidly elevated in response to ETO (Fig. 5B), confirming its apparent involvement in a
17 generic ATM-mediated DNA damage response [61,62]. By 60 min, we also observed
18 reduced levels of pSer142 on DPF2 (Zinc finger protein ubi-d4), a known regulator of the
19 non-canonical NF- κ B pathway [63], and pThr220/221 (site ambiguous) on the RelA binding
20 partner RPS3 (40S ribosomal protein S3), both of which have previously been reported to be
21 elevated in HEK293 cells following 3 h UV exposure [52]. Although binding of RSP3 to RelA
22 is thought to enhance its ability to bind DNA *in vitro* [64], RSP3 functions as a negative
23 regulator of H₂O₂-mediated DNA repair [65]. It is possible therefore that pThr220/221 on
24 RPS3, and pSer142 on DPF2, serve to modulate the RelA transcriptional complexes and/or
25 the consensus promoter regions for NF- κ B binding, that are required for DNA repair in
26 response to HU.

27

28 Using NetPhorest [41,42], we were able to predict possible kinase-substrate relationships for
29 46% (77 out of 167) of the 'class I' phosphosites ($ptmRS \geq 0.75$) that were regulated in
30 response to HU (Fig. 6E). CK2 α 2 was predicted as the kinase responsible for the vast
31 majority (27 out of 43) of the phosphosites reduced in response to HU, based on the
32 prevalence of acidic residues C-terminal to the site of phosphorylation (in particular at +3)
33 clearly evident in the sequence analysis (Fig. 6F). Consequently, HU might have significant
34 effects on CK2 α 2 (or other acidophilic kinases) that feed into the RelA-mediated DNA
35 damage response. Prevalent among both up- and down-regulated phosphosites were
36 predicted substrates of the cyclin-dependent kinases (CDK1/2/3/5 group) which, together
37 with the prediction of substrates for ERK1 (MAPK3) and p38 α (MAPK14), contributes to the
38 enrichment of Pro at the +1 position in both the HU up- and down-regulated phosphosites

1 (Fig. 6F and 5G). Also among the up-regulated phosphopeptides are a number of predicted
2 ATM substrates which, whilst only representing a small proportion of the total number of HU-
3 regulated phosphosites, corresponds with the small enrichment for Gln in the +1 position
4 among the up-regulated phosphosites. (Fig. 6E and 6G).

5

6 Comparing the putative kinase-mediated regulation of substrates for those differentially
7 regulated phosphopeptides in the RelA interactome in response to the two different types of
8 DNA damaging agents revealed some interesting observations: although ATM-predicted
9 substrates were enhanced with both ETO and HU, over twice as many putative substrates
10 were elevated with ETO. Predicted substrates for CK2 α 2 are prevalent in the differentially
11 regulated (both up- and down-) phosphosites under both conditions, although HU induces a
12 far greater reduction in levels of putative CK2 α 2 substrates than ETO. In contrast, putative
13 substrates for the dual specificity protein kinase CLK1, which has a role in regulating
14 alternative splicing, are notably elevated in response to HU (Fig. 6E), but not particularly with
15 ETO (Fig. 5E). Interestingly, binding sites for 14-3-3 ϵ , which generally conform to the
16 RXXpS/TXP consensus, were elevated under both conditions, but particularly in response to
17 HU. 14-3-3 proteins are known to be involved in the cellular response to DNA damage; 14-3-
18 3 ϵ in particular, modulates NF- κ B signalling in part by virtue of its ability to bind
19 phosphorylated TAK1 (and its cognate phosphatase PPM1B), and thereby regulate its anti-
20 apoptotic capabilities [66,67]. In response to DNA damage stress, this manifests as inhibition
21 of the anti-apoptotic activity of TAK1, promoting an apoptotic phenotype that is enhanced by
22 the 14-3-3 ϵ -mediated disruption of DP-2 from the E2F transcriptional complex [68]. The fact
23 that we observe elevated putative 14-3-3 ϵ binding sites following HU treatment (but
24 significantly less so with ETO), is in agreement with the pro-apoptotic response of HU-
25 treated cells. Consequently, we hypothesise that the ability of components of the RelA
26 interactome to bind 14-3-3 ϵ may be a driving factor in achieving the expected cell
27 death/survival phenotype in response to these two DNA damaging agents.

1 DISCUSSION

2 Protein phosphorylation is a key reversible, dynamic PTM that rapidly governs protein
3 complex formation, particularly of transcription factor complexes, thereby coupling
4 extracellular stressors with compensatory transcriptional output. To understand the role of
5 phosphorylation in regulating the RelA transcriptional network in response to different types
6 of DNA damage, we used a quantitative phosphoproteomics to explore the dynamics of the
7 phosphorylated RelA interactome in response to either ETO or HU. Evaluating the RelA
8 network under these conditions is pertinent, given the central role of this transcription factor
9 in directing the cellular response towards either senescence or apoptosis. Exposure of
10 U2OS cells to either ETO or HU had very limited effect on the phosphorylated RelA
11 interactome; only 246 of the 815 RelA interacting phosphoproteins that we identified in total
12 changed upon treatment. Of these, less than 1% were specific to the type of DNA stress,
13 with 7 or 8 unique proteins (respectively) being identified in the RelA network following
14 exposure of U2OS cells to either the DSB-inducing ETO or to HU. However, although there
15 was little change in the make-up of this network, there was evidence of subtle, but
16 significant, changes in the phosphorylation states of the RelA bound proteins as a function of
17 both the type of and duration of the DNA damaging agent used. Not only did the anti-
18 apoptotic agent ETO invoke a more rapid cellular response than HU, both in terms of
19 maximal H2AX levels (Fig. 1B), and quantifiable changes in phosphopeptide levels (Figs. 4,
20 5 and 6; Supp. Tables 2 & 3), but interestingly this study pointed to the differential regulation
21 of key cellular processes and the involvement of unique signalling pathways in modulating
22 the treatment-specific functions of RelA.

23
24 Examination of the RelA network hub (the bait) revealed two novel phosphorylation events
25 amongst the RelA phosphopeptides that we were able to identify and quantify in this trypsin-
26 based peptide analysis: Thr54 and Ser169, both of which are within the DNA binding
27 domain. However, only Ser45 and Ser131 were statistically differentially regulated in
28 response to either ETO or HU. While Ser131 was statistically elevated upon treatment with
29 ETO at 120 min, the fold change was marginal (1.03-fold), with similar fold change (1.05-
30 fold) being observed for this phosphosite in response to HU, albeit at a shorter 30 min
31 point. The RelA peptide containing pSer45 was unchanged upon ETO treatment, and was
32 statistically downregulated by 60 min exposure to HU, again with low (1.05) fold change.
33 Given that we were evaluating the total cellular pool of RelA, rather than specifically the
34 nuclear portion where we would expect *e.g.* Ser45 phosphorylation to have a greater
35 regulatory effect [26], it is perhaps not surprising that the phosphopeptide changes
36 quantified in this study were relatively low.

1 A number of our findings of regulated phosphorylation site changes are in agreement with
2 other published studies. However, the overall fold change in phosphopeptide levels across
3 this study were relatively low (maximally 1.7 fold), and speaks to the necessity to avoid,
4 wherever possible, implementation of a fold-change cut-off during this type of analysis.
5 While ETO-regulated RelA bound phosphoproteins were primarily involved in transcription,
6 cell division and mitosis, and DSB repair (as might be expected), HU-mediated changes
7 were predominantly observed in proteins with functions in rRNA and mRNA processing, and
8 translational initiation. Where changes were observed, ETO predominantly resulted in
9 elevated phosphopeptide levels, with a number of the ETO-regulated phosphorylation sites
10 identified having been reported previously to be modulated in response to either IR or UV
11 radiation. It was interesting to note that transcriptional regulation and DNA damage repair
12 proteins were enriched in those datasets with both elevated and reduced phosphopeptide
13 levels, suggesting coordinated regulation of these processed through different effectors in
14 response to DSB. In addition to the involvement in AMT/ATR signalling previously reported,
15 potential substrates for which were much more prevalent following ETO treatment than HU,
16 kinase substrate prediction suggested roles for CDKs and ERK1 (or their cognate
17 phosphatases), in regulating RelA complexes in response to ETO. In contrast, levels of the
18 activation loop phosphopeptide in MAPK1/ERK2, traditionally thought to be a marker of
19 kinase activity, were elevated in response to HU, but not ETO, suggesting differential MAPK
20 isoform signalling in response to these two types of DNA damage. The prediction of
21 substrates for p38 α in the regulated phosphorylation sites following cellular exposure to HU
22 (but not ETO), also points to a potential HU-specific regulation of this stress activated protein
23 kinase. Finally, our data point to a role for 14-3-3 ϵ binding propensity in facilitating the
24 cellular response to HU, which may be a contributing factor in differentiating the pro-and
25 anti-apoptotic phenotypes that are the result of prolonged cellular exposure to these two types
26 of DNA damaging agents, and we believe is worthy of further investigation.

27

28

29

30

31

32

33

34

35

36

1
2
3
4
5
6
7
8
9
10
11
12
13
14
15
16
17
18
19
20
21
22
23
24
25
26
27
28
29
30
31
32

Author Contributions

CEE and NDP obtained funding. AC, CFF and CEE designed the experiments and analysed the data, with bioinformatics support from SP, AK and ARJ. LS generated the HA-RelA U2OS cell line. CFF treated the cells, prepared the samples and did the immunoblotting studies. AC, CFF and PJB performed the MS analysis. EC performed the RelA CoIPs. AC and CEE wrote the paper with contributions from all authors, who also approved the final version prior to submission.

Funding Sources

This work was supported by the Biotechnology and Biological Sciences Research Council (BBSRC; BB/L009501/1 to CEE and NDP, BB/R000182/1 and BB/M012557/1 to CEE) and Cancer Research UK (CRUK; C1443/A22095 to NDP and CEE, and C1443/A12750 to NDP).

Notes

The authors declare no competing financial interest. The mass spectrometry proteomics data have been deposited to the ProteomeXchange Consortium via the PRIDE partner repository with the dataset identifiers PXD019587 and PXD019589.

Abbreviations

AGC, automatic gain control; CID, collision-induced dissociation; DSB, double strand break; ETD, electron-transfer dissociation; ETcaD, electron transfer with supplemental collision activation; EThcD, electron-transfer higher energy collisional dissociation; ETO, etoposide; GO, gene ontology; HCD, higher energy collisional dissociation; HU, hydroxyurea; IR, ionizing radiation; MS, mass spectrometry; PD, Proteome Discoverer; PTM, post-translational modification; RHD, Rel homology domain; TD, transactivation domain; UV, ultraviolet.

1 REFERENCES

- 2 1 Perkins, N. D. (2012) The diverse and complex roles of NF- κ B subunits in cancer.
3 Nat. Rev. Cancer **12**, 121–132.
- 4 2 Christian, F., Smith, E. and Carmody, R. (2016) The Regulation of NF- κ B Subunits by
5 Phosphorylation. Cells **5**, 12.
- 6 3 Lu, X. and Yarbrough, W. G. (2015) Negative regulation of RelA phosphorylation:
7 Emerging players and their roles in cancer. Cytokine Growth Factor Rev., Elsevier Ltd
8 **26**, 7–13.
- 9 4 Giridharan, S. and Srinivasan, M. (2018) Mechanisms of NF- κ B p65 and strategies for
10 therapeutic manipulation. J. Inflamm. Res. **11**, 407–419.
- 11 5 Kumar, A., Takada, Y., Boriek, A. M. and Aggarwal, B. B. (2004) Nuclear factor- κ B: Its
12 role in health and disease. J. Mol. Med. **82**, 434–448.
- 13 6 Kim, H. J., Hawke, N. and Baldwin, A. S. (2006) NF- κ B and IKK as therapeutic targets
14 in cancer. Cell Death Differ. **13**, 738–747.
- 15 7 Didonato, J. A., Mercurio, F. and Karin, M. (2012) NF- κ B and the link between
16 inflammation and cancer. Immunol. Rev. **246**, 379–400.
- 17 8 Tilstra, J. S., Niedernhofer, L. J., Paul, D., Tilstra, J. S., Robinson, A. R., Wang, J.,
18 Gregg, S. Q., Clauson, C. L., Reay, D. P., Nasto, L. A., et al. (2012) NF- κ B inhibition
19 delays DNA damage – induced senescence and aging in mice Find the latest version :
20 NF- κ B inhibition delays DNA damage – induced senescence and aging in mice **122**,
21 2601–2612.
- 22 9 Wang, J., Jacob, N. K., Ladner, K. J., Beg, A., Perko, J. D., Tanner, S. M.,
23 Liyanarachchi, S., Fishel, R. and Guttridge, D. C. (2009) RelA/p65 functions to
24 maintain cellular senescence by regulating genomic stability and DNA repair. EMBO
25 Rep., Nature Publishing Group **10**, 1272–1278.
- 26 10 Chien, Y., Scuoppo, C., Wang, X., Fang, X., Balgley, B., Bolden, J. E., Premssirut, P.,
27 Luo, W., Chicas, A., Lee, C. S., et al. (2011) Control of the senescence-associated
28 secretory phenotype by NF- κ B promotes senescence and enhances chemosensitivity.
29 Genes Dev. **25**, 2125–2136.
- 30 11 Slater, M. L. (1973) Effect of reversible inhibition of deoxyribonucleic acid synthesis
31 on the yeast cell cycle. J. Bacteriol. **113**, 263–270.
- 32 12 Krakoff, I. H., Brown, N. C. and Reichard, P. (1968) Inhibition Reductase of
33 Ribonucleoside by Hydroxyurea1 Diphosphate 1559–1565.
- 34 13 Stauber, R. H., Knauer, S. K., Habtemichael, N., Bier, C., Unruhe, B., Weisheit, S.,
35 Spange, S., Nonnenmacher, F., Fetz, V., Ginter, T., et al. (2012) A combination of a
36 ribonucleotide reductase inhibitor and histone deacetylase inhibitors downregulates
37 EGFR and triggers BIM-dependent apoptosis in head and neck cancer. Oncotarget **3**,
38 31–43.

- 1 14 Murai, J. and Pommier, Y. (2019) Phosphatase 1 Nuclear Targeting Subunit, a Novel
2 DNA Repair Partner of PARP1. *Cancer Res.* **79**, 2460–2461.
- 3 15 Krämer, O. H., Knauer, S. K., Zimmermann, D., Stauber, R. H. and Heinzl, T. (2008)
4 Histone deacetylase inhibitors and hydroxyurea modulate the cell cycle and
5 cooperatively induce apoptosis. *Oncogene* **27**, 732–740.
- 6 16 Pommier, Y., Leo, E., Zhang, H. and Marchand, C. (2010) DNA topoisomerases and
7 their poisoning by anticancer and antibacterial drugs. *Chem. Biol., Elsevier Ltd* **17**,
8 421–433.
- 9 17 Montecucco, A. and Biamonti, G. (2007) Cellular response to etoposide treatment.
10 *Cancer Lett.* **252**, 9–18.
- 11 18 Montecucco, A., Zanetta, F. and Biamonti, G. (2015) Molecular mechanisms of
12 etoposide. *EXCLI J.* **14**, 95–108.
- 13 19 Schäfer, C., Göder, A., Beyer, M., Kiweler, N., Mahendrarajah, N., Rauch, A.,
14 Nikolova, T., Stojanovic, N., Wieczorek, M., Reich, T. R., et al. (2017) Class I histone
15 deacetylases regulate p53/NF- κ B crosstalk in cancer cells. *Cell. Signal., Elsevier Inc.*
16 **29**, 218–225.
- 17 20 Schneider, G., Henrich, A., Greiner, G., Wolf, V., Lovas, A., Wieczorek, M., Wagner,
18 T., Reichardt, S., Von Werder, A., Schmid, R. M., et al. (2010) Cross talk between
19 stimulated NF- κ B and the tumor suppressor p53. *Oncogene* **29**, 2795–2806.
- 20 21 Wagner, T., Kiweler, N., Wolff, K., Knauer, S. K., Brandl, A., Hemmerich, P.,
21 Dannenberg, J. H., Heinzl, T., Schneider, G. and Krämer, O. H. (2015) Sumoylation
22 of HDAC2 promotes NF- κ B-dependent gene expression. *Oncotarget* **6**, 7123–7135.
- 23 22 Wu, Z. H. and Miyamoto, S. (2008) Induction of a pro-apoptotic ATM-NF- κ B pathway
24 and its repression by ATR in response to replication stress. *EMBO J.* **27**, 1963–1973.
- 25 23 Perkins, N. D. (2006) Post-translational modifications regulating the activity and
26 function of the nuclear factor kappa B pathway. *Oncogene* **25**, 6717–6730.
- 27 24 Li, H., Wittwer, T., Weber, A., Schneider, H., Moreno, R., Maine, G. N., Kracht, M.,
28 Schmitz, M. L. and Burstein, E. (2012) Regulation of NF- κ B activity by competition
29 between RelA acetylation and ubiquitination. *Oncogene* **31**, 611–623.
- 30 25 Huang, B., Yang, X. D., Lamb, A. and Chen, L. F. (2010) Posttranslational
31 modifications of NF- κ B: Another layer of regulation for NF- κ B signalling pathway. *Cell.*
32 *Signal.* **22**, 1282–1290.
- 33 26 Lanucara, F., Lam, C., Mann, J., Monie, T. P., Colombo, S. A. P., Holman, S. W.,
34 Boyd, J., Dange, M. C., Mann, D. A., White, M. R. H., et al. (2016) Dynamic
35 phosphorylation of RelA on Ser42 and Ser45 in response to TNF a stimulation
36 regulates DNA binding and transcription. *Open Biol.* **6**, 160055.
- 37 27 Chen, L.-F., Williams, S. A., Mu, Y., Nakano, H., Duerr, J. M., Buckbinder, L. and
38 Greene, W. C. (2005) NF- κ B RelA Phosphorylation Regulates RelA Acetylation. *Mol.*

1 Cell. Biol. **25**, 7966–7975.

2 28 Nihira, K., Ando, Y., Yamaguchi, T., Kagami, Y., Miki, Y. and Yoshida, K. (2010) Pim-
3 1 controls NF- κ B signalling by stabilizing RelA/p65. *Cell Death Differ.* **17**, 689–698.

4 29 Campbell, K. J., Witty, J. M., Rocha, S. and Perkins, N. D. (2006) Cisplatin mimics
5 ARF tumor suppressor regulation of RelA (p65) nuclear factor- κ B transactivation.
6 *Cancer Res.* **66**, 929–935.

7 30 Msaki, A., Sánchez, A. M., Koh, L. F., Barré, B., Rocha, S., Perkins, N. D. and
8 Johnson, R. F. (2011) The role of RelA (p65) threonine 505 phosphorylation in the
9 regulation of cell growth, survival, and migration. *Mol. Biol. Cell* **22**, 3032–3040.

10 31 Ferries, S., Perkins, S., Brownridge, P. J., Campbell, A., Evers, P. A., Jones, A. R.
11 and Evers, C. E. (2017) Evaluation of Parameters for Confident Phosphorylation Site
12 Localization Using an Orbitrap Fusion Tribrid Mass Spectrometer. *J. Proteome Res.*
13 **16**, 3448–3459.

14 32 Chawade, A., Alexandersson, E. and Levander, F. (2014) Normalyzer: A Tool for
15 Rapid Evaluation of Normalization Methods for Omics Data Sets. *J. Proteome Res.*
16 **13**, 3114–3120.

17 33 Huber, W., Von Heydebreck, A., Sültmann, H., Poustka, A. and Vingron, M. (2002)
18 Variance stabilization applied to microarray data calibration and to the quantification
19 of differential expression. *Bioinformatics* **18**.

20 34 Mellacheruvu, D., Wright, Z., Couzens, A. L., Lambert, J. P., St-Denis, N. A., Li, T.,
21 Miteva, Y. V., Hauri, S., Sardi, M. E., Low, T. Y., et al. (2013) The CRAPome: A
22 contaminant repository for affinity purification-mass spectrometry data. *Nat. Methods*
23 **10**, 730–736.

24 35 Szklarczyk, D., Gable, A. L., Lyon, D., Junge, A., Wyder, S., Huerta-Cepas, J.,
25 Simonovic, M., Doncheva, N. T., Morris, J. H., Bork, P., et al. (2019) STRING v11:
26 Protein-protein association networks with increased coverage, supporting functional
27 discovery in genome-wide experimental datasets. *Nucleic Acids Res.* **47**, 607–613.

28 36 Shannon, P., Markiel, A., Ozier, O., Baliga, N. S., Wang, J. T., Ramage, D., Amin, N.,
29 Schwikowski, B. and Ideker, T. (2001) Cytoscape: A Software Environment for
30 Integrated Models. *Genome Res.* **13**, 426.

31 37 Huang, D. W., Sherman, B. T. and Lempicki, R. A. (2009) Bioinformatics enrichment
32 tools: Paths toward the comprehensive functional analysis of large gene lists. *Nucleic
33 Acids Res.* **37**, 1–13.

34 38 Huang, D. W., Sherman, B. T. and Lempicki, R. A. (2009) Systematic and integrative
35 analysis of large gene lists using DAVID bioinformatics resources. *Nat. Protoc.* **4**, 44–
36 57.

37 39 Supek, F., Bošnjak, M., Škunca, N. and Šmuc, T. (2011) Revigo summarizes and
38 visualizes long lists of gene ontology terms. *PLoS One* **6**.

1 40 Kuznetsova, I., Lugmayr, A., Siira, S. J., Rackham, O. and Filipovska, A. (2019)
2 CirGO: an alternative circular way of visualising gene ontology terms. *BMC*
3 *Bioinformatics*, *BMC Bioinformatics* **20**, 84.

4 41 Horn, H., Schoof, E. M., Kim, J., Robin, X., Miller, M. L., Diella, F., Palma, A.,
5 Cesareni, G., Jensen, L. J. and Linding, R. (2014) KinomeExplorer: An integrated
6 platform for kinome biology studies. *Nat. Methods*, Nature Publishing Group **11**, 603–
7 604.

8 42 Miller, M. L., Lars Juhl Jensen, Diella, F., Jørgensen, C., Tinti, M., Li, L., Hsiung, M.,
9 Parker, S. A., Bordeaux, J., Sicheritz-Ponten, T., et al. (2008) Linear Motif Atlas for
10 Phosphorylation-Dependent Signalling. *Sci. Signal.* **1**.

11 43 Colaert, N., Helsens, K., Martens, L., Vandekerckhove, J. and Gevaert, K. (2009)
12 Improved visualization of protein consensus sequences by iceLogo. *Nat. Methods*,
13 Nature Publishing Group **6**, 786–787.

14 44 Kuo, L. J. and Yang, L. X. (2008) γ -H2AX- A novel biomaker for DNA double-strand
15 breaks. *In Vivo (Brooklyn)*. **22**, 305–310.

16 45 Ward, I. M. and Chen, J. (2001) Histone H2AX Is Phosphorylated in an ATR-
17 dependent Manner in Response to Replicational Stress. *J. Biol. Chem.* **276**, 47759–
18 47762.

19 46 Anderson, L. A. and Perkins, N. D. (2003) Regulation of RelA (p65) Function by the
20 Large Subunit of Replication Factor C. *Mol. Cell. Biol.* **23**, 721–732.

21 47 Perkins, N. D., Felzien, L. K., Betts, J. C., Leung, K., Beach, D. H. and Nabel, G. J.
22 (1997) Regulation of NF- κ B by cyclin-dependent kinases associated with the p300
23 coactivator. *Science (80-)*. **275**, 523–527.

24 48 Perkins, N. D., Agranoff, A. B., Pascal, E. and Nabel, G. J. (1994) An interaction
25 between the DNA-binding domains of RelA(p65) and Sp1 mediates human
26 immunodeficiency virus gene activation. *Mol. Cell. Biol.* **14**, 6570–6583.

27 49 Girdwood, D., Bumpass, D., Vaughan, O. A., Thain, A., Anderson, L. A., Snowden, A.
28 W., Garcia-Wilson, E., Perkins, N. D. and Hay, R. T. (2003) p300 transcriptional
29 repression is mediated by SUMO modification. *Mol. Cell* **11**, 1043–1054.

30 50 Zhang, B., Wu, J., Cai, Y., Luo, M., Wang, B. and Gu, Y. (2018) AAED1 modulates
31 proliferation and glycolysis in gastric cancer. *Oncol. Rep.* **40**, 1156–1164.

32 51 Matsuoka, S., Ballif, B. A., Smogorzewska, A., McDonald, E. R., Hurov, K. E., Luo, J.,
33 Bakalarski, C. E., Zhao, Z., Solimini, N., Lerenthal, Y., et al. (2007) ATM and ATR
34 substrate analysis reveals extensive protein networks responsive to DNA damage.
35 *Science (80-)*. **316**, 1160–1166.

36 52 Boeing, S., Williamson, L., Encheva, V., Gori, I., Saunders, R. E., Instrell, R., Aygün,
37 O., Rodriguez-Martinez, M., Weems, J. C., Kelly, G. P., et al. (2016) Multiomic
38 Analysis of the UV-Induced DNA Damage Response. *Cell Rep.* **15**, 1597–1610.

- 1 53 Nicolai, S., Mahen, R., Raschellà, G., Marini, A., Pieraccioli, M., Malewicz, M.,
2 Venkitaraman, A. R. and Melino, G. (2020) ZNF281 is recruited on DNA breaks to
3 facilitate DNA repair by non-homologous end joining. *Oncogene*, Springer US **39**,
4 754–766.
- 5 54 Enserink, J. M. and Kolodner, R. D. (2010) An overview of Cdk1-controlled targets
6 and processes. *Cell Div.* **5**, 1–41.
- 7 55 Gonzalez, F. A., Raden, D. L. and Davis, R. J. (1991) Identification of substrate
8 recognition determinants for human ERK1 and ERK2 protein kinases. *J. Biol. Chem.*
9 **266**, 22159–22163.
- 10 56 Fang, L., Choudhary, S., Zhao, Y., Edeh, C. B., Yang, C., Boldogh, I. and Brasier, A.
11 R. (2014) ATM regulates NF- κ B-dependent immediate-early genes via RelA ser 276
12 phosphorylation coupled to CDK9 promoter recruitment. *Nucleic Acids Res.* **42**, 8416–
13 8432.
- 14 57 Traven, A. and Heierhorst, J. (2005) SQ/TQ cluster domains: Concentrated ATM/ATR
15 kinase phosphorylation site regions in DNA-damage-response proteins. *BioEssays*
16 **27**, 397–407.
- 17 58 Roskoski, R. (2012) ERK1/2 MAP kinases: Structure, function, and regulation.
18 *Pharmacol. Res.*, Elsevier Ltd **66**, 105–143.
- 19 59 Cargnello, M. and Roux, P. P. (2011) Activation and Function of the MAPKs and Their
20 Substrates, the MAPK-Activated Protein Kinases. *Microbiol. Mol. Biol. Rev.* **75**, 50–
21 83.
- 22 60 Wang, Y., Xu, J., Gao, G., Li, J., Huang, H., Jin, H., Zhu, J., Che, X. and Huang, C.
23 (2016) Tumor-suppressor NF κ B2 p100 interacts with ERK2 and stabilizes PTEN
24 mRNA via inhibition of MIR-494. *Oncogene* **35**, 4080–4090.
- 25 61 Gatei, M., Young, D., Cerosaletti, K. M., Desai-Mehta, A., Spring, K., Kozlov, S.,
26 Lavin, M. F., Gatti, R. A., Concannon, P. and Khanna, K. K. (2000) ATM-dependent
27 phosphorylation of nibrin in response to radiation exposure. *Nat. Genet.* **25**, 115–119.
- 28 62 Wu, X., Ranganathan, V., Weisman, D. S., Heine, W. F., Ciccone, D. N., Neill, T. B.
29 O., Crick, K. E., Pierce, K. A., Lane, W. S., Rathbun, G., et al. (2000) ATM
30 phosphorylation of Nijmegen breakage syndrome protein is required in a DNA
31 damage response. *Nature* **405**, 477–482.
- 32 63 Tando, T., Ishizaka, A., Watanabe, H., Ito, T., Iida, S., Haraguchi, T., Mizutani, T.,
33 Izumi, T., Isobe, T., Akiyama, T., et al. (2010) Requiem protein links RelB/p52 and the
34 Brm-type SWI/SNF complex in a noncanonical NF- κ B pathway. *J. Biol. Chem.* **285**,
35 21951–21960.
- 36 64 Mulero, M. C., Shahabi, S., Ko, M. S., Schiffer, J. M., Huang, D. Bin, Wang, V. Y. F.,
37 Amaro, R. E., Huxford, T. and Ghosh, G. (2018) Protein Cofactors Are Essential for
38 High-Affinity DNA Binding by the Nuclear Factor κ B RelA Subunit. *Biochemistry* **57**,

- 1 2943–2957.
- 2 65 Hegde, V., Yadavilli, S. and Deutsch, W. A. (2007) Knockdown of ribosomal protein
3 S3 protects human cells from genotoxic stress. *DNA Repair (Amst)*. **6**, 94–99.
- 4 66 Pennington, K., Chan, T., Torres, M. and Andersen, J. (2018) The dynamic and
5 stress-adaptive signalling hub of 14-3-3: emerging mechanisms of regulation and
6 context-dependent protein–protein interactions. *Oncogene, Springer US* **37**, 5587–
7 5604.
- 8 67 Zuo, S., Xue, Y., Tang, S., Yao, J., Du, R., Yang, P. and Chen, X. (2010) 14-3-3
9 epsilon dynamically interacts with key components of mitogen-activated protein
10 kinase signal module for selective modulation of the TNF- α -Induced time course-
11 dependent NF- κ b activity. *J. Proteome Res.* **9**, 3465–3478.
- 12 68 Milton, A. H., Khaire, N., Ingram, L., O'Donnell, A. J. and La Thangue, N. B. (2006)
13 14-3-3 Proteins integrate E2F activity with the DNA damage response. *EMBO J.* **25**,
14 1046–1057.
- 15
- 16

1 **Tables**

2

3

Treatment	UniProt ID	Protein Name
Etoposide	Q86U06	Probable RNA-binding protein 23
	O96013	Serine/threonine-protein kinase PAK 4
	P27361	Mitogen-activated protein kinase 3
	Q8WYH8	Inhibitor of growth protein 5
	Q9BXP5	Serrate RNA effector molecule homolog
	Q7RTV5	Peroxiredoxin-like 2C
	Q99956	Dual specificity protein phosphatase 9
Hydroxyurea	Q9BY44	Eukaryotic translation initiation factor 2A
	Q8N3F8	MICAL-like protein 1
	Q4G0J3	La-related protein 7
	O94979	Protein transport protein Sec31A
	Q12931	Heat shock protein 75 kDa, mitochondrial
	E9PRG8	Uncharacterized protein C11orf98
	O75113	NEDD4-binding protein 1
	P12270	Nucleoprotein TPR

4

5 **Table 1. DNA damage specific RelA binding partners.** Proteins identified as binding HA-
 6 RelA in the presence of either etoposide or hydroxyurea are listed.

1 Figure Legends

2
3 **Figure 1. Workflow for evaluation of DNA damage response of HA-RelA U2OS cells with either Etoposide (ETO) or Hydroxyurea (HU).** (A) HA-RelA U2OS cells were treated with either 0.1% DMSO (control), ETO (50 μ M) or HU (2 mM) for the times indicated to induce DNA damage. (B) Following treatment with either ETO or HU, HA-RelA U2OS cell lysates were immunoblotted with antibodies against either γ H2AX as a marker of DNA damage, or RelA/p65. (C) Workflow for evaluation of the phosphorylated RelA interactome. Cells were treated as in (A), and RelA-bound proteins immunoprecipitated with an anti-HA antibody. Proteins were subjected to tryptic digestion and TiO₂-based phosphopeptide enrichment. (D) Peptides were analysed by LC-MS/MS using a QExactive HF and subjected to label-free quantification following appropriate normalisation.

13
14 **Figure 2. Network map of RelA interacting phosphoproteins.** Proteins from phosphopeptides quantified following HA-RelA immunoprecipitation in control (0.1% DMSO control), ETO (50 μ M) or HU (2 mM) treated U2OS cells were evaluated with STRING (v11.0) [35] for prior experimental evidence of interaction. Kmeans clustering was used to identify the top 9 enriched GO clusters of biological function and plotted using Cytoscape [36]. The shape of the nodes represent the conditions under which they was identified: round nodes represents proteins identified across all conditions; diamond nodes indicate proteins unique to ETO treatment; square nodes indicate proteins unique to HU treatment. (A) red nodes represent those proteins mapped to IKK/NF- κ B signalling; (B) dark green nodes represent those proteins mapped to DNA damage response/DNA repair; (C) blue nodes represent those proteins mapped to repression of gene expression; (D) yellow nodes represent those proteins mapped to transcriptional regulation; (E) pink nodes represent those proteins mapped to mRNA processing/splicing; (F) violet nodes represent those proteins mapped to ribosome biogenesis/rRNA processing; (G) light green nodes represent those proteins mapped to cell division/mitosis; (H) purple nodes represent those proteins mapped to MAPK/VEGF signalling. Proteins outside of these 8 enriched clusters have nodes in grey. The outline colour of the nodes within the 8 clusters shows proteins with differentially regulated phosphopeptides following treatment with either ETO (blue), HU (red), or both (black).

33
34 **Figure 3. Co-immunoprecipitation of PAK4 with RelA increases following cellular treatment with etoposide.** HA-RelA or HA control U2OS cells were treated with either ETO (50 μ M) or HU (2 mM) for the times indicated to induce DNA damage. Total cell extracts (inputs, left) or HA-RelA immunoprecipitated samples (α HA IP, right) were then analysed by western blot with antibodies against either PAK4, RelA or KPNB1 (as a loading control). Data are representative of three independent experiments.

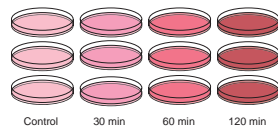
40
41
42 **Figure 4. Etoposide and Hydroxyurea induced different phosphorylation dynamics in the RelA network.** GO term biological process enrichment was examined for all phosphopeptides exhibiting a statistically significant change in response to either (A) etoposide (ETO) or (B) hydroxyurea (HU). (C) Overlap of those proteins with significant change in phosphopeptide abundance at one or more time points with ETO or HU. (D) Distribution of phosphopeptide changes between sustained, dynamic and late responders for ETO vs HU treatment, where 'Late Responders' indicates a change at 120 minutes only, 'Sustained' indicates a change at 30 or 60 minutes which is sustained throughout, and 'Dynamic' indicates a change at 30 or 60 minutes which is reversed. (E, F) Heatmaps of the

1 fold change in phosphopeptide levels following treatment with either ETO (**E**) or HU (**F**) at
2 30, 60 or 120 min relative to control levels. Hierarchical row clustering was performed on the
3 \log_2 fold changes.
4

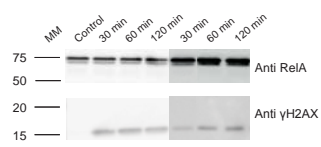
5 **Figure 5. Etoposide-mediated phosphopeptides changes in the RelA network.** Volcano
6 plots showing fold changes in phosphopeptide abundance following Bayesian statistical
7 analysis to evaluate significant differences as a function of (**A**) 30 min, (**B**) 60 min or (**C**) 120
8 min treatment with ETO. \log_2 -fold change are presented as a function of the $-\log_2$ p-value;
9 differentially down-regulated (red) or up-regulated (blue) phosphopeptides with a p-value
10 ≤ 0.05 are highlighted. Select data points are annotated with their protein accession number
11 and site of phosphorylation. Phosphopeptides observed upon ETO treatment, but not in the
12 control extracts are not reported here. (**D**) GO term enrichment analysis using DAVID of
13 proteins with significantly regulated phosphopeptides in response to ETO (all time points)
14 relative to control. Phosphopeptides with a Benjamini-Hochberg adjusted p-value ≤ 0.05 are
15 labelled. BP = biological process (green); CC = cellular compartment (yellow); MF =
16 molecular function (purple); UP = UniProt keyword (pink). (**E**) NetPhorest kinase-substrate
17 prediction for significantly down- (red) or up-regulated (blue) phosphosites. IceLogo
18 sequence analysis of (**F**) down-regulated or (**G**) up-regulated phosphosites.

19
20 **Figure 6. Hydroxyurea-mediated phosphopeptides changes in the RelA network.**
21 Volcano plots showing fold changes in phosphopeptide abundance following Bayesian
22 statistical analysis to evaluate significant differences as a function of (**A**) 30 min, (**B**) 60 min
23 or (**C**) 120 min treatment with HU. \log_2 -fold change are presented as a function of the $-\log_2$
24 p-value; differentially down-regulated (red) or up-regulated (blue) phosphopeptides with a p-
25 value ≤ 0.05 are highlighted. Select data points are annotated with their protein accession
26 number and site of phosphorylation. Phosphopeptides observed upon HU treatment, but not
27 in the control extracts are not reported here. (**D**) GO term enrichment analysis using DAVID
28 of proteins with significantly regulated phosphopeptides in response to HU (all time points)
29 relative to control. Phosphopeptides with a Benjamini-Hochberg adjusted p-value ≤ 0.05 are
30 labelled. BP = biological process (green); CC = cellular compartment (yellow); MF =
31 molecular function (purple); UP = UniProt keyword (pink). (**E**) NetPhorest kinase-substrate
32 prediction for significantly down- (red) or up-regulated (blue) phosphosites. IceLogo
33 sequence analysis of (**F**) down-regulated or (**G**) up-regulated phosphosites.
34

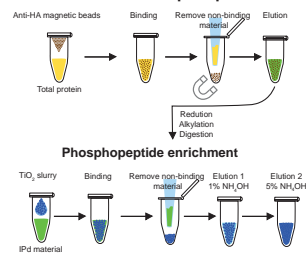
A Etoposide/Hydroxyurea treatment



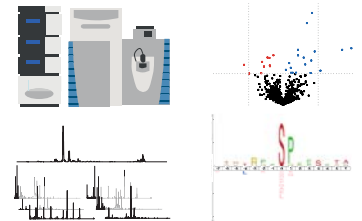
B Etoposide Hydroxyurea

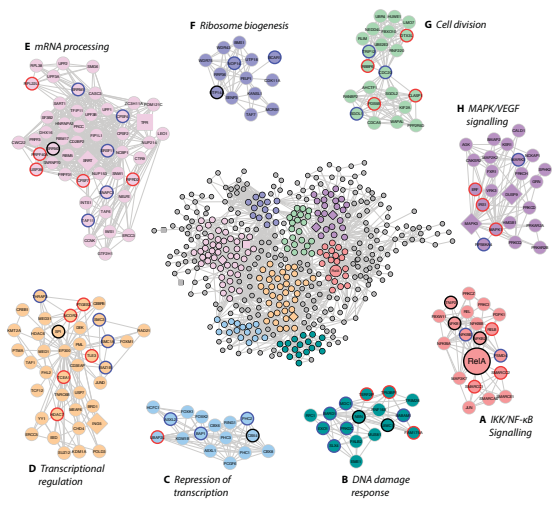


C HA-RelA Immunoprecipitation



D LC-MS/MS





HA control cells

HA-RelA cells

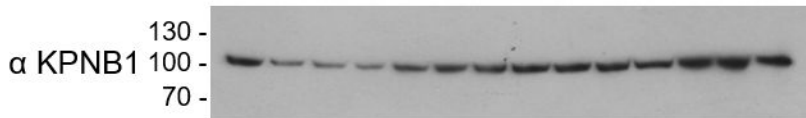
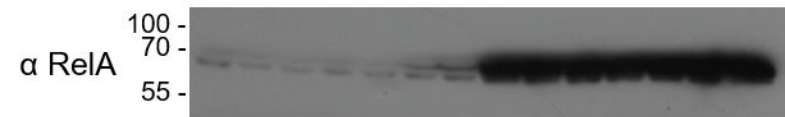
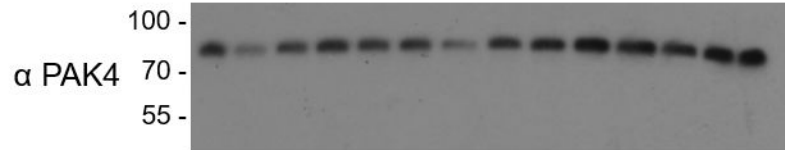
HA control cells

HA-RelA cells

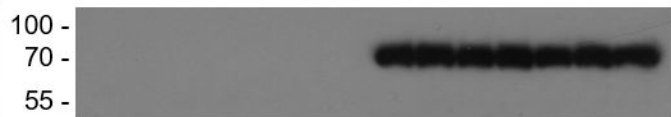
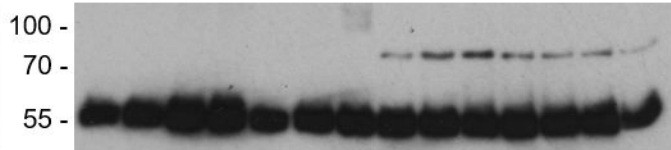
ETO
(mins)HU
(mins)ETO
(mins)HU
(mins)ETO
(mins)HU
(mins)ETO
(mins)HU
(mins)*Antibody*

0 30 60 120 30 60 120 0 30 60 120 30 60 120

0 30 60 120 30 60 120 0 30 60 120 30 60 120



Inputs

 α HA IP

